Preparation and Properties of the Highly Porous Poly(ethylene-*co*-vinyl alcohol)/Multiwalled Carbon Nanotube Nanocomposites Prepared by a Simple Saponification Method

Eun-Ju Lee,[1] Jin-San Yoon,[1] Eun-Soo Park[2]

[1]*Department of Polymer Science and Engineering, Inha University, Incheon 402-751, Korea*
[2]*Youngchang Silicone Co., Ltd., 481-7, Gasan-Dong, Kumchun-Gu, Seoul 153-803, Korea*

Received 1 December 2010; accepted 24 November 2011
DOI 10.1002/app.36537
Published online 17 February 2012 in Wiley Online Library (wileyonlinelibrary.com).

ABSTRACT: Multiwalled carbon nanotubes (MWNTs) were functionalized by electron-beam (EB) irradiation in air at room temperature. As the EB dose was increased to 1000 kGy, Fourier transform infrared analysis detected the formation of carbonyl groups in the irradiated MWNTs. Poly(ethylene-*co*-vinyl alcohol)/MWNT nanocomposite particles were prepared by the incorporation of EB-irradiated MWNTs in a poly(ethylene-*co*-vinyl acetate) (EVA)/toluene solution and saponification in an ethanol/KOH solution. Scanning electron microscopy observation showed that the nanocomposite particles had a highly porous, spongelike structure of connected matrix polymers and MWNTs. At low EVA/MWNT concentrations, the particles were less porous, and the precipitated polymer phase had a granular structure. At high concentrations, the porosity increased, and the precipitated polymer phase became spongelike. The thermal and mechanical properties and the electrical resistivity change of the prepared nanocomposites were investigated. © 2012 Wiley Periodicals, Inc. J Appl Polym Sci 125: E691–E704, 2012

Key words: electron beam irradiation; copolymers; morphology; nanocomposites

INTRODUCTION

Poly(ethylene-*co*-vinyl alcohol) (EVOH) copolymers are a semicrystalline polymer regardless of vinyl alcohol (VOH) content and are easily prepared by the saponification of poly(ethylene-*co*-vinyl acetate) (EVA).[1,2] EVOH copolymers have been widely used in the food packaging, biomedical, and pharmaceutical industries because of their excellent gas-barrier properties, high resistance to oils, good mechanical strength, and harmlessness to health.[2,3] They also have excellent hydrophilicity and moisture-absorbing/releasing properties unlike conventional synthetic polymers; this is a consequence of their —OH side groups. Thereby, EVOH has significant potential as a polymeric filler or inorganic filler surface modifier. Generally, fillers are bulk components in various detergents with a primary role of modifying and altering the physical properties of a material. They are commonly compounded with synthetic polymer resins or emulsions as extenders and provide opacity, color, mechanical strength, hardness, and other additional functionalities.[4–6]

Porous functionalized polymeric fillers can be produced by a phase-inversion method.[7] This causes separation of the homogeneous polymer solution into a solid polymer and a liquid solvent phase. The precipitated coagulants form a porous structure containing a network of uniform pores. Production parameters that affect the pore structure and properties include the polymer concentration, the precipitation media and temperature, and the amount of solvent and nonsolvent in the polymer solution. These factors can be varied to produce a porous structure with a large range of pore sizes and to alter the chemical, thermal, and mechanical properties.[8] Highly porous polymer materials have found numerous uses in a wide range of commercial products, including absorbents, supports for liquid chromatography, ion-exchange applications, bioseparators, and metal recovery.[7,8]

In this study, EVOH/multiwalled carbon nanotube (MWNT) nanocomposite particles were prepared from an EVA/MWNT/toluene suspension with direct precipitation and alkaline saponification. The MWNTs were functionalized by an electron-beam (EB) irradiation process in air. The morphology, thermal and mechanical properties, and electrical resistivity of the prepared nanocomposites were investigated.

Correspondence to: E.-S. Park (t2phage@hitel.net).
Contract grant sponsor: Small and Medium Enterprises Technology Innovation Program, Republic of Korea.

TABLE I
Characteristics of EVA

Material	Density (g/cm^3)	VAc content (wt %)	Melting temperature (°C)	Melt flow index (g/10 min)
EVA	0.949	28	74	18

EXPERIMENTAL

Materials

MWNTs (CM-95, purity = 95 wt %, average diameter = 15 nm, average length = 20 μm, specific gravity = 1.8, Iljin Nanotech Co., Ltd., Seoul, Korea) and EVA (1159, Hanhwa Chemical Co., Ltd., Seoul, Korea) was used as received. EVA resin and the MWNTs were predried in a convection oven for at least 12 h at 50°C to remove any moisture from the pellets before processing. The characteristics of the resins used in this study are summarized in Table I.

Instrumentation

Scanning electron microscopy (SEM) observations of the nanocomposite samples were performed on a Hitachi model S-4300 (Tokyo, Japan). The fractured surfaces of the nanocomposites were prepared with cryogenic fracturing in liquid nitrogen and were then coated with platinum in a sputter coater. The morphology was determined at an accelerating voltage of 15 kV. The surface sample composition was evaluated with SEM (Hitachi S-4300) equipped with an energy-dispersive X-ray spectroscope.

Elemental analysis (EA) was performed in a Thermo EA1112 apparatus (Thermo Finnigan, Rodano, Italy), and Fourier transform infrared (FTIR) absorption spectra of the samples were measured with a PerkinElmer infrared spectrometer (Spectrum 2000, Shelton, CT) in the wave-number range from 4000 to 400 cm^{-1} and were analyzed with commercial software.

The thermal properties of the samples were determined by differential scanning calorimetry (DSC; PerkinElmer DSC 7, Norwalk, CT). The thermal history of the products was removed by scanning to 180°C at a heating rate of 20°C/min. After the sample was cooled at a rate of −5°C/min to room temperature, it was reheated at 20 to 180°C, and the DSC thermograms were obtained.

TABLE II
Specifications of the ELV-4 EB Accelerator

Energy (MeV)	EB power (kW)	Nonuniformity of current density (%)	Input voltage (V)
0.8–1.5	50	<10	220/380

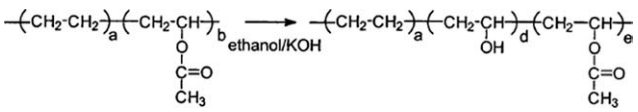

Scheme 1

The thermal stability of the samples was determined by thermogravimetry (PerkinElmer TGS-2). The TGA curves were obtained under an N_2 atmosphere and scanned from 20 to 800°C at a heating rate of 20°C/min.

The hardness of the specimens was measured with a Shore A hardness tester (GS-706, Teclock Co., Kyoto, Japan), and the readings were averaged. Five locations were measured for each specimen and surface.

EB irradiation of the MWNTs

The MWNTs were EB-irradiated in air at room temperature with an EB accelerator (ELV 4, EB Tech Co., Ltd., Daejeon, Korea). Irradiation doses of 400, 800, 1000, and 1200 kGy were used. The specifications of the ELV 4 are presented Table II.

Preparation of the EVOH/electron-beam-irradiated multiwalled carbon nanotube (EB–MWNT) nanocomposites

The EVA pellets (100 g) were first swollen in toluene (900 g) at room temperature for 12 h; this was followed by heating at 60°C for 4 h. The required amount of EB–MWNTs was dispersed in the 10 wt % EVA/toluene solution by mechanical premixing and bath sonication for 2 h. The diluted suspension (20 mL, 5.0 wt % in toluene) was saponified by consecutive dropwise addition to a stirred 200 mL of a KOH/ethanol solution (0.5*M*). The heterogeneous solution was stirred at room temperature (20 ± 2°C) for ambient time; then, the solution was filtered, and the filtrate was washed with methanol. The filtrate was dried *in vacuo* at 60°C to a constant weight (Scheme 1).

Calculation of the percentage saponification

The percentage saponification of EVA was determined from the FTIR absorbance ratio of the methyl groups of the vinyl acetate (VAc) unit (1370 cm^{-1}) and the methylene group of the ethylene unit (720 cm^{-1})[9] with eq. (1). The absorbances at about 1370 and 720 cm^{-1} of the standard EVA film were calculated after baseline correction. The absorbance ratios of standard materials (EVA 1126, VAc content = 9.5 wt %; EVA 1156, VAc content = 15.0 wt %; and EVA1159, VAc content = 28.0 wt %, Hanhwa Chemical Co.) of known composition were plotted against the ratio of the VAc content and ethylene content.

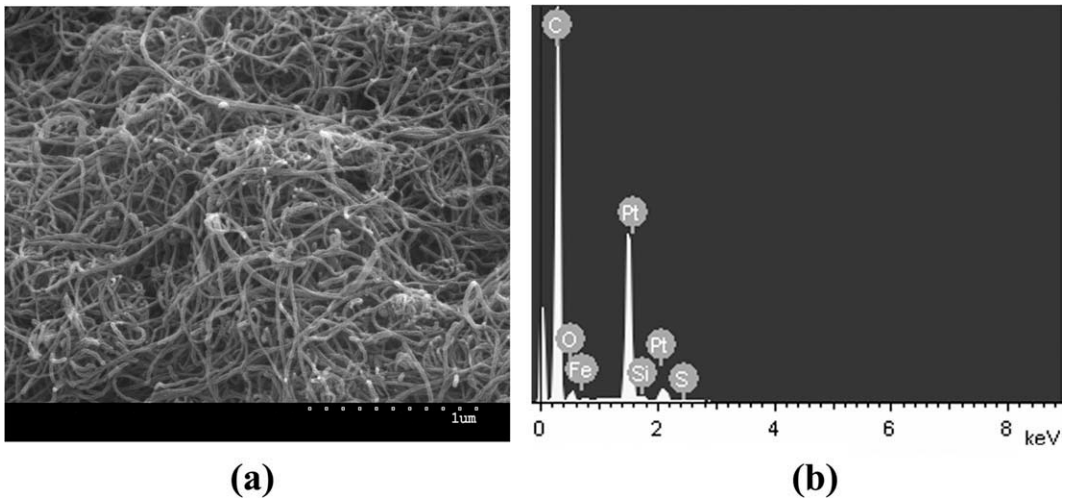

Figure 1 SEM image and EDX analysis results of the pristine MWNTs.

The values were plotted against the corresponding VAc-to-ethylene content ratio. From the calibration graph, the slope and intercept were calculated:

$$Y = 1.6207X + 0.4244 \quad (1)$$

where Y is the absorbance ratio and X is the ratio of VAc to ethylene unit content (A/B). The saponified sample film was held in the magnetic sample holder. The absorbances at about 1370 and 720 cm^{-1} were calculated from the resulting spectra. By knowing X (A/B) and the fact that $A + B = 100$, we calculated the percentage (%) VAc content.

Heterogeneous reaction of EVOH and EB–MWNTs

The saponified EVA/EB–MWNT nanocomposites (2.2 g) were first dissolved in dimethyl sulfoxide at 140°C and kept under an N_2 atmosphere. After the solution was stirred for 30 min, tetrabutyl titanate

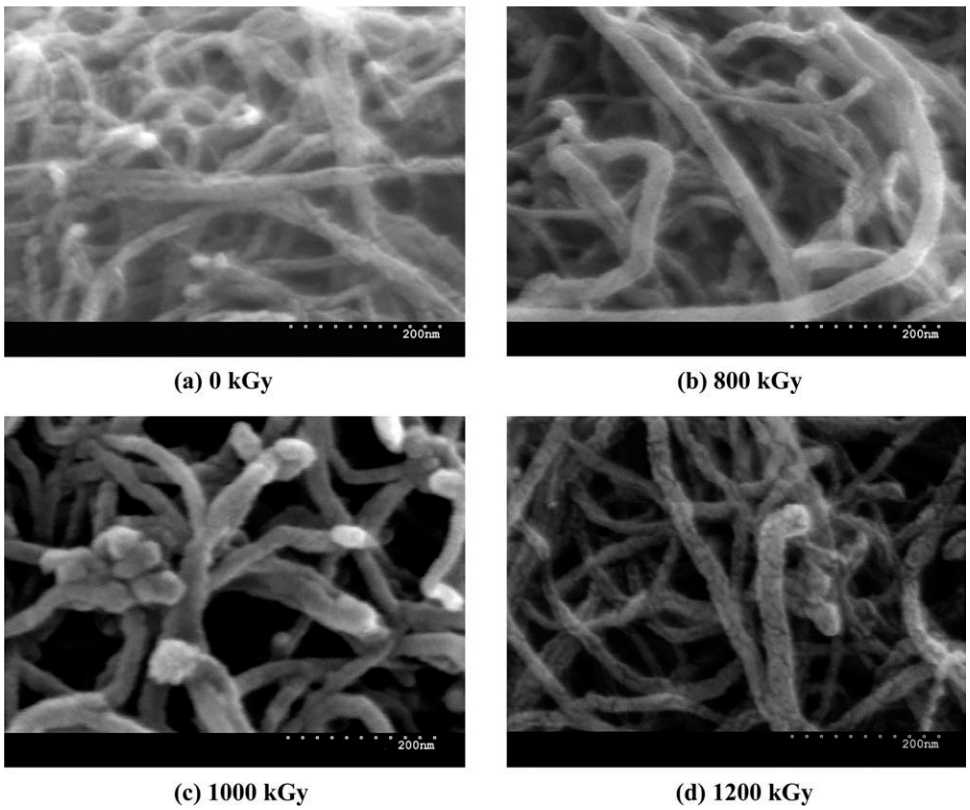

Figure 2 SEM micrographs of the surface morphology of the EB–MWNTs.

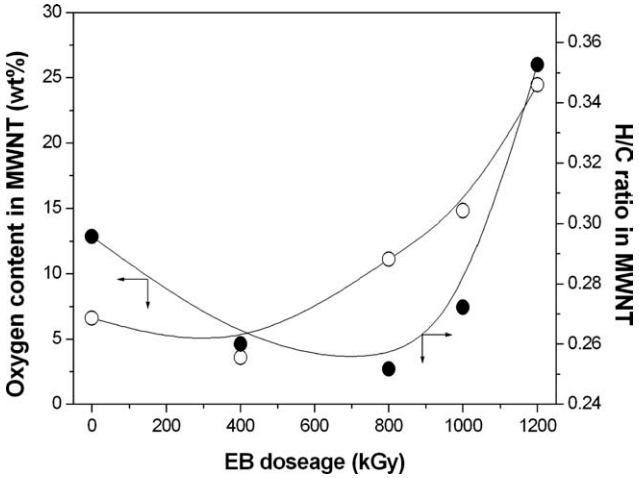

Figure 3 (○, left axis) EDX and (●, right axis) EA analysis results of the EB–MWNTs.

(TNBT; 0.2 mL) was then added to the hot solution, and the solution was stirred for 3 h. The product was precipitated in methanol and dried in a vacuum oven at 60°C.

Tensile test procedure

The saponified EVA/EB–MWNT powder was subsequently hot-pressed into a sheet of uniform thickness (ca. 0.5 mm) with a plate press at 150°C for 10 min under about 5 atm and quickly immersed in water. The sheet thus formed was free from any distortion problems. Dumbbell specimens for the tensile tests were prepared in accordance with the IEC 60811-1-1 specification. The test specimens were preconditioned to 20% relative humidity and 20 ± 1°C to standardize the test conditions. The tensile properties of the samples were determined with a universal testing machine (model DEC-A500TC, Dawha Test Machine, Buchun, Korea) at a crosshead speed of 250 mm/min. The mean value of at least five specimens of each sample was taken, although specimens that broke in an unusual manner were disregarded.

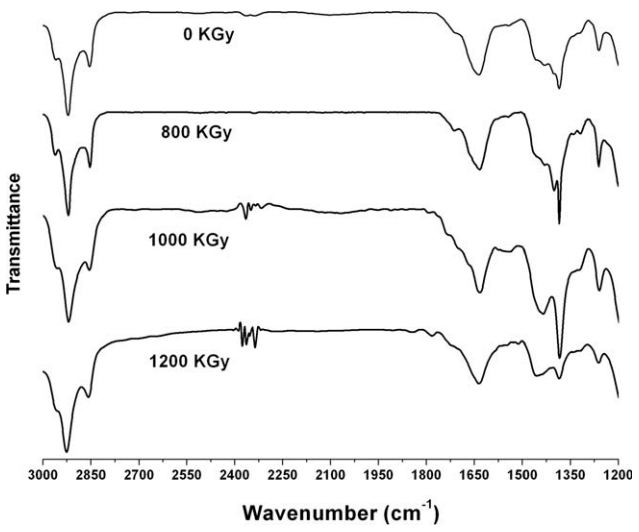

Figure 4 FTIR spectra of the pristine MWNTs and EB–MWNTs.

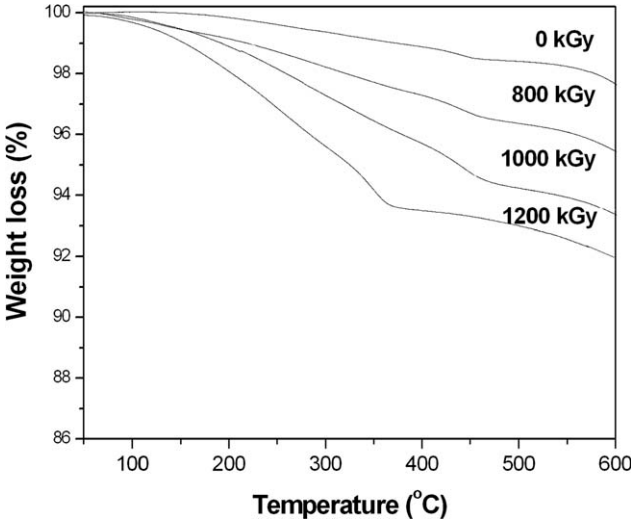

Figure 5 TGA thermograms of the pristine MWNTs and EB–MWNTs.

Measurement of the volume resistivity (ρ_v)

The surface electrical resistance of the EVA/EB–MWNT and EVOH/EB–MWNT films (80 mm length × 10 mm width) was detected by a megohmmeter (TeraOhm 5 kV, Metrel, West Yorkshire, UK) according to ASTM D 257. The charge time was 30 s, and the current stress of the measurements was 2500 V at 20 ± 1°C. ρ_v values of the prepared films were calculated with the following equation:

TABLE III
Tensile Properties of the EVA/EB–MWNT Nanocomposites

Sample code	Tensile properties		Hardness (Shore A)
	Tensile strength (MPa)	Elongation at break (%)	
EVA	10.6 ± 0.9	1472 ± 106	83.6 ± 1.1
EVA/MWNT–1%	10.9 ± 0.6	1242 ± 62	87.4 ± 1.0
EVA/MWNT800–1%	11.4 ± 1.1	1241 ± 91	87.2 ± 0.4
EVA/MWNT1000–1%	11.3 ± 0.8	1359 ± 87	87.6 ± 1.0
EVA/MWNT1200–1%	11.5 ± 0.3	1269 ± 47	87.6 ± 1.0
EVA/MWNT–5%	11.9 ± 0.8	1046 ± 95	90.6 ± 2.0
EVA/MWNT800–5%	12.5 ± 1.2	1111 ± 40	90.8 ± 1.3
EVA/MWNT1000–5%	12.6 ± 0.4	1294 ± 69	90.4 ± 1.0
EVA/MWNT1200–5%	12.7 ± 1.2	1167 ± 92	90.2 ± 0.0
EVA/MWNT–10%	11.2 ± 1.3	146 ± 12	92.4 ± 1.0
EVA/MWNT800–10%	12.8 ± 1.0	133 ± 23	92.0 ± 2.0
EVA/MWNT1000–10%	13.0 ± 1.7	102 ± 27	92.0 ± 1.0
EVA/MWNT1200–10%	13.7 ± 0.8	125 ± 18	92.2 ± 1.0

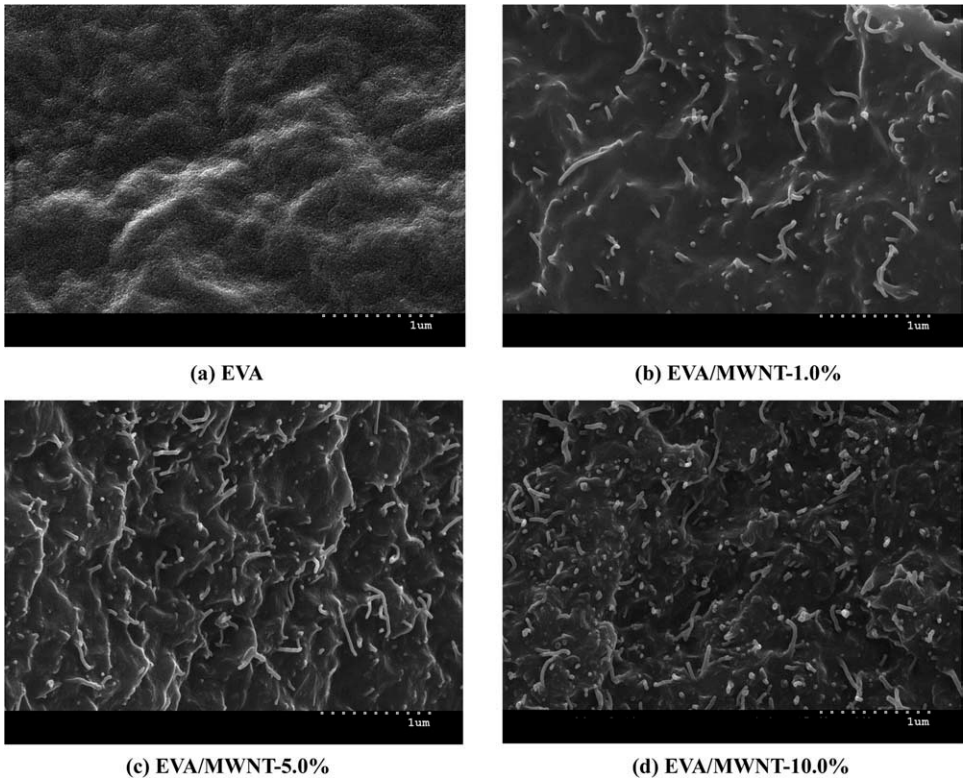

Figure 6 Fracture surfaces of the hot-pressed EVA/MWNT nanocomposites containing 0.0, 1.0, 5.0, and 10.0 wt % pristine MWNTs.

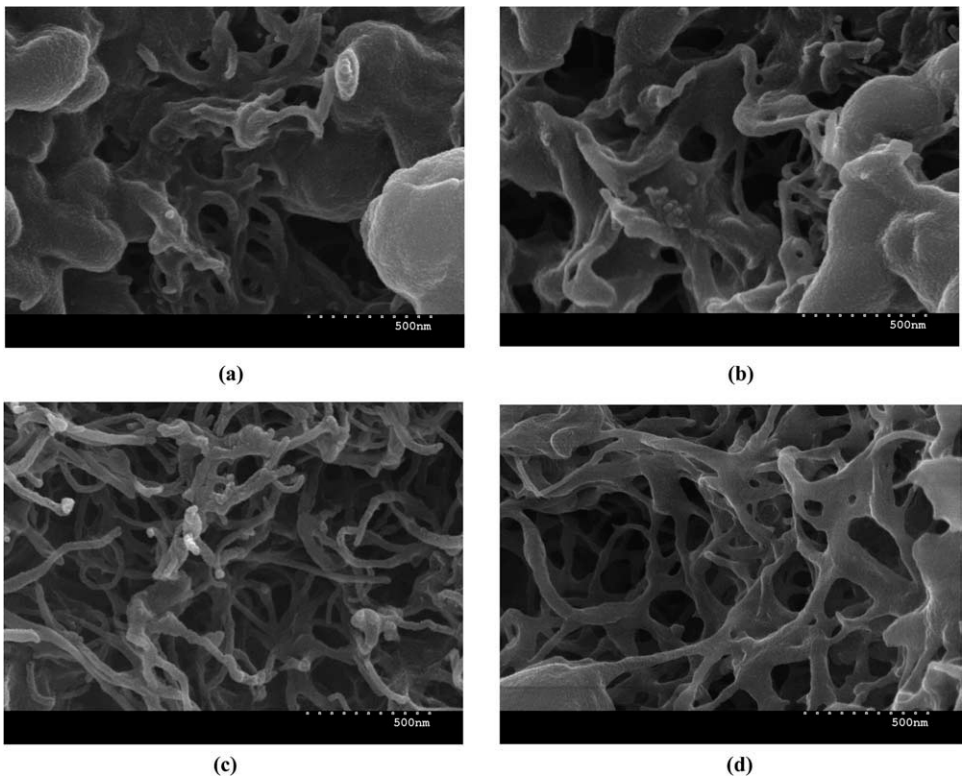

Figure 7 SEM micrographs of the saponified EVA/MWNT coagulants at various EVA/MWNT suspension concentrations: (a) 0.5, (b) 1.0, (c) 1.25, and (d) 2.5 wt % in toluene.

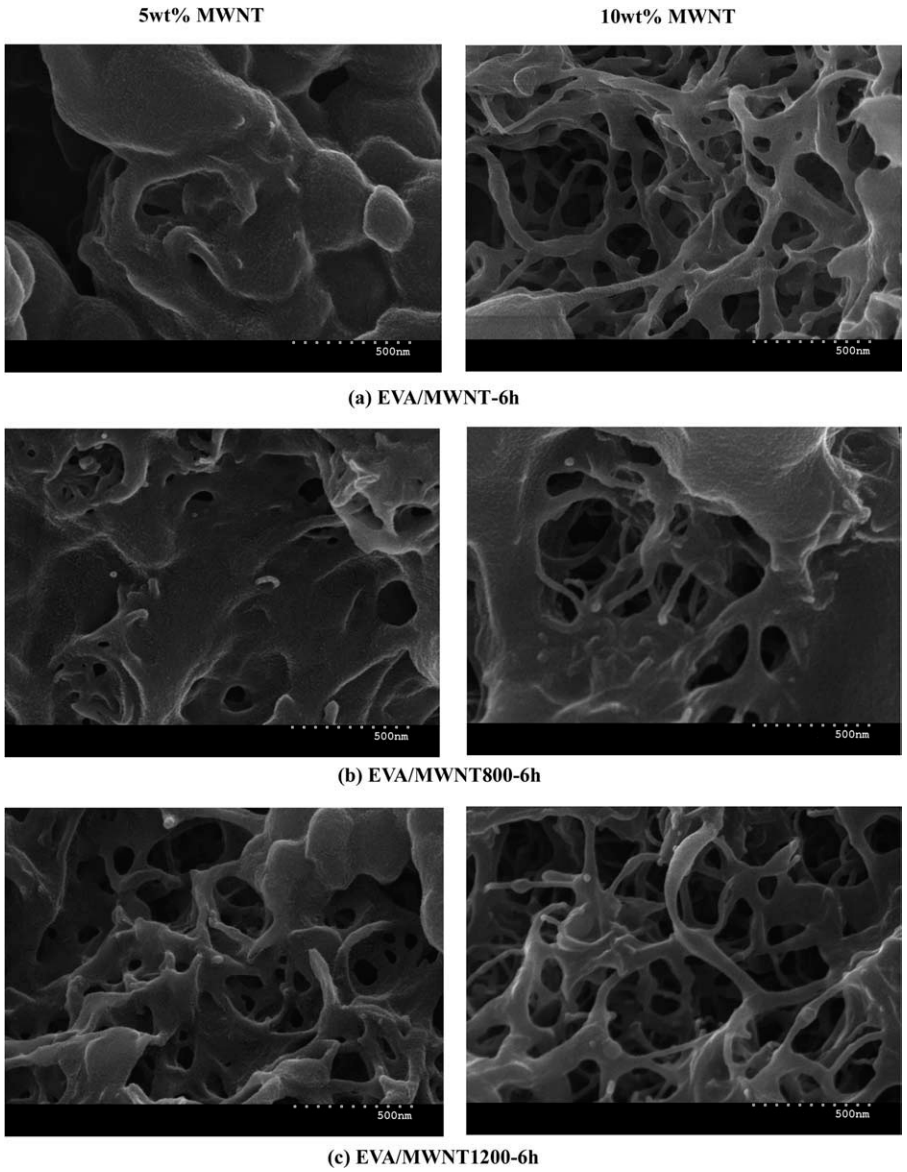

Figure 8 SEM micrographs of the saponified EVA/MWNT and EVA/EB–MWNT coagulants.

$$\rho_v = \frac{AR_v}{L} \quad (2)$$

where A, R_v, and L represent the area of the effective electrode (cm^2), the measured resistance (Ω), and the distance between electrodes (cm), respectively.

RESULTS AND DISCUSSION

EB irradiation effect of the MWNTs

Figure 1 shows the SEM image and energy-dispersive X-ray spectroscopy (EDX) analysis results of the MWNTs produced by a chemical vapor deposition process without any purification. The average diameter and length of the MWNTs were approximately 15 nm and 20–50 μm, respectively. The as-received MWNTs contained some impurities and entangled into a bulk piece. The EDX results of the pristine MWNTs showed small peaks that corresponded to Fe, Si, and S, respectively. The Si peak had its origin in the silicon substrate, whereas the other peaks were due to the precursor gases present in the gas mixture and the catalyst. Carbon nanotubes (CNTs) are often formed in entangled ropes with 10–100 CNTs per bundle, depending on the method of synthesis. They can be produced by a number of methods: direct-current arc discharge, laser ablation, and a thermal and plasma-enhanced chemical vapor deposition process.[10] The method of production affects the level of purity of the MWNTs. Impurities exist as catalysis particles, amorphous, carbons and nontubular fullerenes.[11] The Pt peaks were due to the platinum sputtering process during SEM sample preparation.

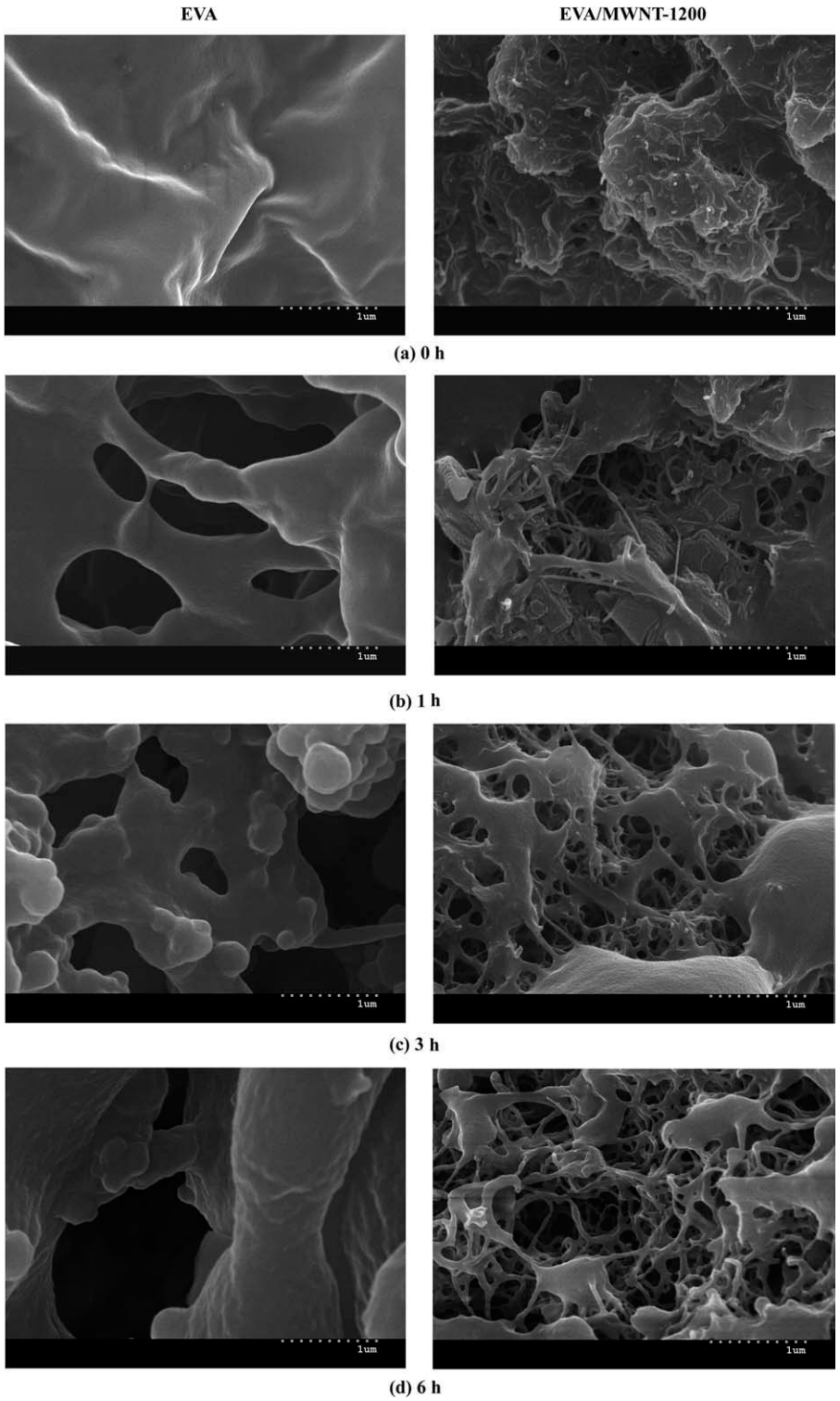

Figure 9 SEM images of the EVA and EVA/MWNT coagulant surfaces prepared with an ethanol/KOH solution with the saponification time.

Figure 2 shows an SEM image of the MWNTs after treatment with EB irradiation. As shown in Figure 2(a), the pristine MWNTs had a relatively smooth surface without extra phases or stains attached to their sidewalls. Although the EB irradiation was increased up to 1000 kGy [Fig. 2(b,c)], the surface appearance of the EB–MWNT did not changed compared to that of the pristine MWNTs. After 1200 kGy of EB irradiation [Fig. 2(d)], the smooth surface disappeared, many wrinkled structures were formed, and the surface roughness increased. In general, the surface of the synthesized

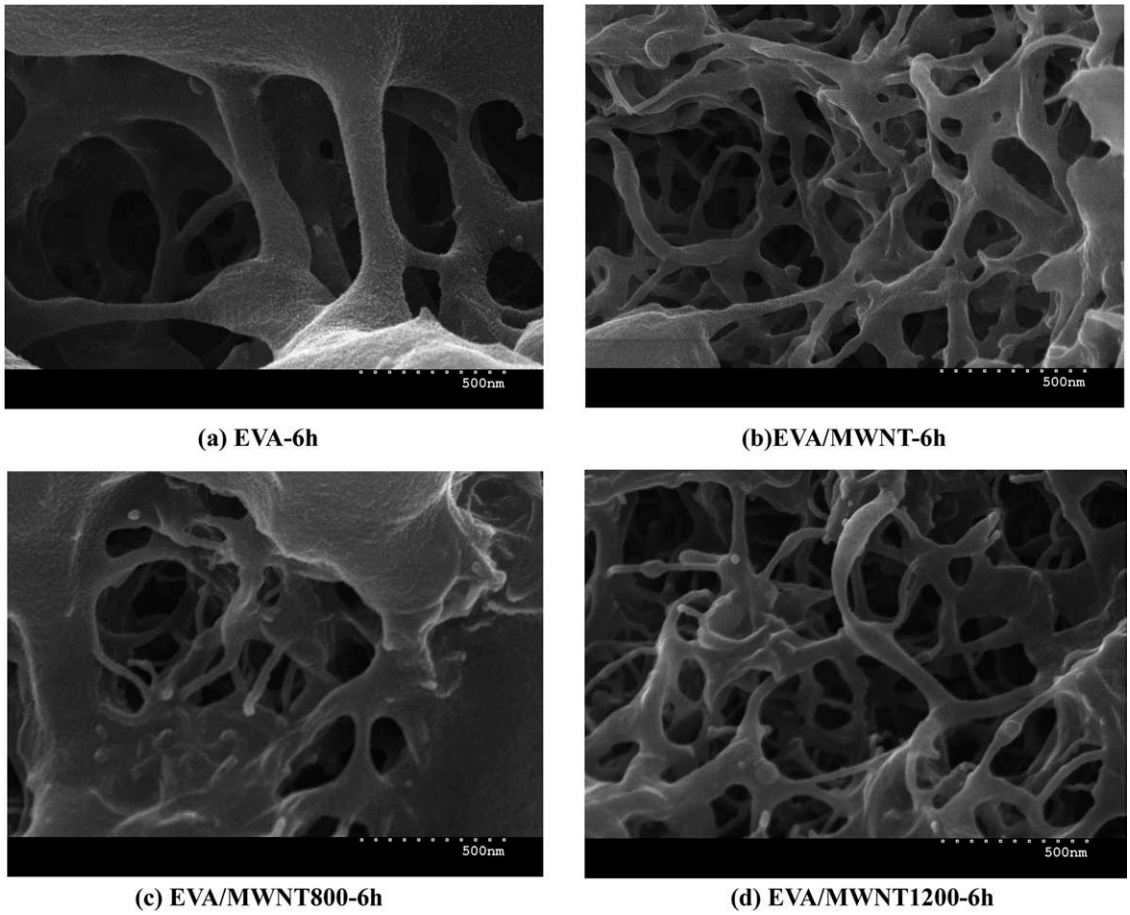

Figure 10 SEM micrographs of the EVA/MWNT and EVA/EB–MWNT coagulants.

CNTs was smooth and relatively defect-free. However, stresses induced Stone Wales transformations, which resulted in the formation of heptagons and concave areas of deformation on the nanotubes.[10]

EA presented (Fig. 3, right axis) a decrease in the hydrogen/carbon (H/C) ratio up to 1000 kGy. After the 1200 kGy irradiation, the H/C ratio was significantly increased. This indicated that the low irradiation dose cleaned the MWNT surface of impurities, according to the SEM and EA results, but the increase in the irradiation doses could have affected the surface roughness and chemical composition.

TABLE IV
Composition and Percentage Saponification of the EVA in the Ethanol/KOH Solution

Sample code	Saponification time (h)	VAc content (wt %)	Saponification (%)
EVA–0 h	0	28.0	—
EVA–0.5 h	0.5	13.2	52.9
EVA–1 h	1	8.5	69.6
EVA–3 h	3	5.2	81.4
EVA–6 h	6	3.2	88.6
EVA–12 h	12	2.8	90.0
EVA–24 h	24	2.5	91.1

The pristine MWNTs and EB–MWNTs were further characterized by FTIR spectroscopy. As it can be seen in Figure 4, the pristine MWNTs and the EB–MWNTs exhibited peaks of C—C bond stretching in the range 3000–2800 cm^{-1}. The broad band at about 3400 cm^{-1} (data not shown) was attributed to the presence of —OH groups on the surface of the MWNTs and was believed to result from ambient atmospheric moisture tightly bound to the MWNTs. The FTIR spectra of the MWNTs after EB irradiation of more than 1000 kGy showed new peaks at 1782 cm^{-1} due to the C=O bond resulting from C=O stretching of the carbonyl group. EDX analysis also confirmed that the oxygen content in the MWNTs increased significantly after irradiation at 1000 kGy (Fig. 3, left axis).

TGA measurements were also conducted on the EB–MWNTs to elucidate their thermal degradation behaviors. As shown in Figure 5, the pristine MWNTs did not show any discernible thermal degradation, with only 2 wt % degradation at 600°C. On the contrary, the weight loss of the EB–MWNTs significantly increased with increasing irradiation dose because of the possible destruction of the CNT structure.[12] Nitric acid or other oxidizing media, such as ozone or oxygen plasma, have been reported to be effective for the partial surface oxidation of CNTs.[13]

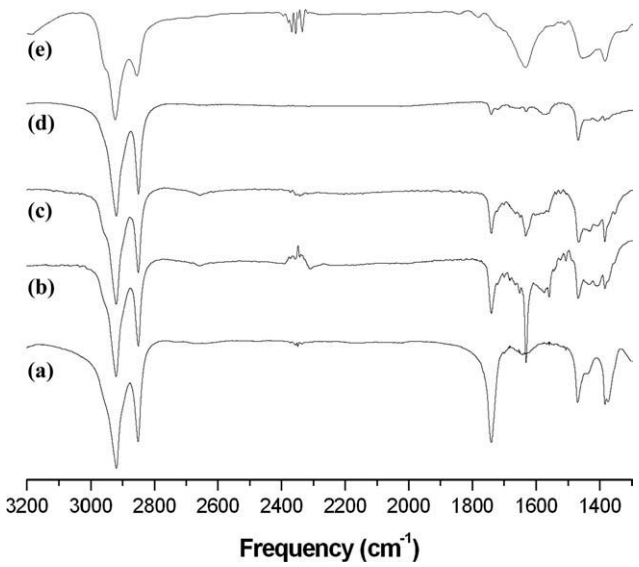

Figure 11 FTIR spectra of the EVA/MWNT1200–10%–6 h nanocomposites along with that of its corresponding saponification time: (a) 0, (b) 1, (c) 3, and (d) 6 h and (e) MWNT1200.

It has been shown that the basal planes of graphite are attacked by molecular oxygen only at their periphery or at defect sites, such as edge planes and vacancies.[14]

Mechanical properties and morphological analysis of the EVA/MWNT nanocomposites

Table III demonstrates the tensile properties and hardness of the EVA/EB–MWNT nanocomposites. The abbreviation of the sample code in Table III, EVA/MWNT800-1%, for example, means that the content of EB–MWNT with a dose of 800 KGy in the nanocomposite was 1 wt%. The tensile strength increased slightly when the pristine MWNT content was increased from 1 to 5 wt %, whereas a further increment showed a significant decrease in the tensile strength. This meant that when the pristine MWNT content was at a value of 10 wt %, the MWNTs did not disperse uniformly, and they formed agglomerations in the polymer matrix. The addition of 10 wt % of the pristine MWNTs enhanced the tensile strength of EVA by 5.7%, whereas this addition to MWNT800, MWNT1000, and MWNT1200 increased it by 16.0, 22.6, and 29.2%, respectively. In general, several factors that influence the dispersion of CNTs in a polymer matrix have to be considered in the preparation process of polymer/CNT nanocomposites. The entanglement of CNTs during the growth process and the attraction between CNTs by van der Waals forces make CNTs themselves tend to aggregate. These factors prevent CNTs from being well dispersed within polymers. The obtained nanocomposites were poor in their mechanical performance, and the intrinsic properties of higher CNTs containing nanocomposites could not be achieved.

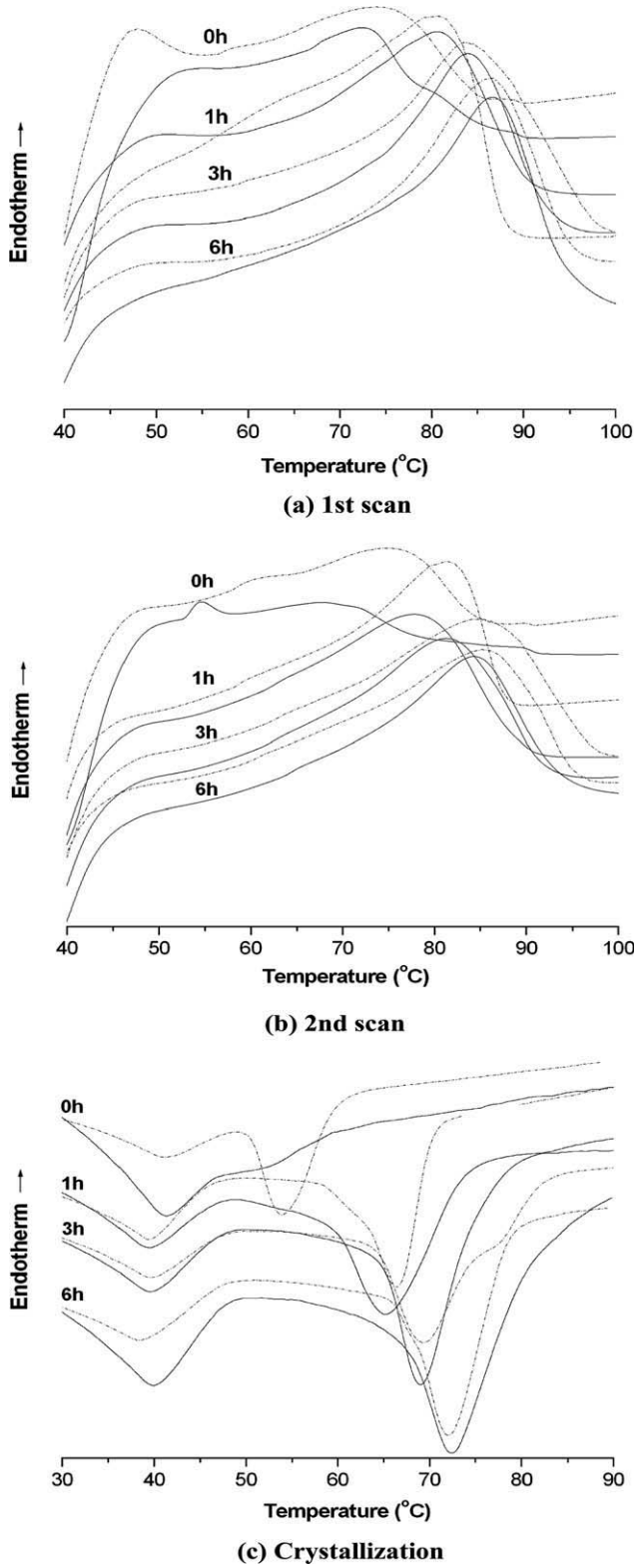

Figure 12 DSC thermograms of the EVA and EVA/MWNT1200–10% nanocomposite as a function of the saponification time: (···) EVA and (—) EVA/MWNT1200–10%–6 h.

TABLE V
DSC Thermal Properties of the Saponified EVA and EVA/MWNT Nanocomposites

	Thermal properties			
	Melting temperature		Crystallization	
Sample code	T_{m1} (first-scan, °C)	T_{m2} (second-scan, °C)	T_c (°C)	$-\Delta H_c$ (J/g)
EVA	73.8	73.9	54.0	21.2
EVA–1 h	80.9	81.9	67.2	28.9
EVA–3 h	83.5	84.1	69.5	38.3
EVA–6 h	86.7	85.1	72.3	42.8
EVA/MWNT1200–10%	72.9	67.9	52.6	17.6
EVA/MWNT1200–10%–1 h	80.2	77.7	65.3	25.3
EVA/MWNT1200–10%–3 h	83.7	80.4	68.7	32.9
EVA/MWNT1200–10%–6 h	86.5	84.1	72.0	38.2

In sharp contrast, the elongation at break of the EVA/MWNT and EVA/EB–MWNT nanocomposites decreased with the presence of filler; this indicated interference by the filler with the mobility or deformability of the matrix.[15] An increase in the weight percentage of filler reduced the deformability of the matrix and, in turn, reduced the ductility in the skin area so that the composite tended to form a weak structure. All nanocomposites increased the hardness in direct relation to the filler content. The hardness is a surface property related to the resistance of a material to local deformation. Increased filler levels resulted in trends toward the reduction of the deformability of the matrix.

Figure 6 shows the fracture surfaces of hot-pressed samples containing 0.0, 1.0, 5.0, and 10.0 wt % MWNTs. Smooth fracture surfaces without the formation of necking were observed for all composites. It could be seen that the fibers were randomly oriented and distributed well in the EVA matrix up to contents of 5 wt %, whereas composites containing 10 wt % showed the presence of few filler aggregations.

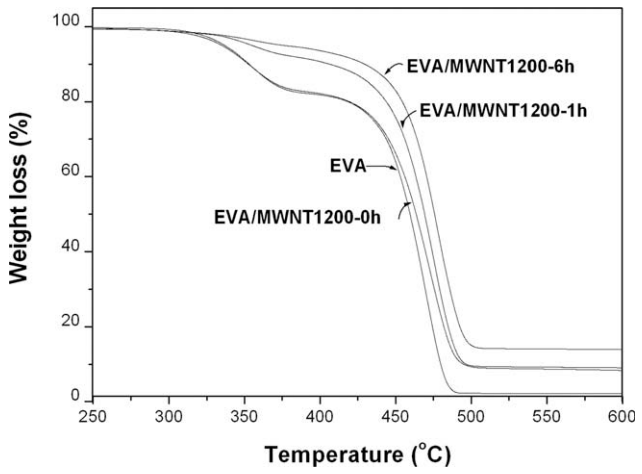

Figure 13 TGA thermograms of the EVA and EVA/MWNT1200–10% nanocomposites.

Porous structure of the saponified EVA/MWNT nanocomposites

Highly porous EVA/MWNT nanocomposite particles were created by the precipitation of the EVA/MWNT/toluene suspension in an ethanol/KOH solution; this saponified the VAc groups in EVA selectively. The approximate size of the saponified particles was 30–50 μm. Figures 7 and 8 show the surfaces of the saponified EVA/MWNT and EVA/EB–MWNT coagulants, respectively. After the coagulant was rinsed off and dried, spongelike structures in the connected matrix polymer and MWNTs were obtained. At low EVA/MWNT suspension concentrations [Fig. 7(a,b)], the particles were less porous, and the precipitated polymer phase had a granular structure consisting of aggregates of precipitated polymer micelles. At high concentrations, the void porosity was increased, and the precipitated polymer phase became a spongelike structure [Fig. 7(c,d)]. Also, the average pore size and number of the particles increased with the MWNT content in suspension (Fig. 8).

Figure 9 shows the SEM images of the EVA and EVA/MWNT coagulant surfaces prepared with the ethanol/KOH solution with the saponification time. The surface of the EVA coagulant [Fig. 9(a)] showed a dense skin layer, which appeared to be nonporous. The formation of the skin layer and the lack of an interconnected pore structure were likely due to the rapid precipitation, where the rate of interdiffusion depended on the value of the solubility parameters of the solvent and nonsolvent. In sharp contrast, small pores could be seen on the surface of the of the EVA/MWNT coagulant. As the saponification time increased, the EVA and EVA/MWNT nanocomposite formed a porous structure containing a network of open-cell pores at the nanometer length scale. The pore size was obtained by direct image analysis from higher magnification SEM micrographs (Fig. 10). The pore sizes of EVA/EB–MWNTs saponified for 6 h ranged between 50 and 200 nm without regard to the EB irradiation dose.

TABLE VI
Tensile Properties of the EVA/MWNT Nanocomposites after Hydrolysis

Sample code	Tensile properties		Hardness (Shore A)
	Tensile strength (MPa)	Elongation at break (%)	
EVA/MWNT–10%–6 h	16.7 ± 0.6	741 ± 55	96.4 ± 1.0
EVA/MWNT800–10%–6 h	18.8 ± 1.1	731 ± 24	96.2 ± 0.4
EVA/MWNT1000–10%–6 h	18.1 ± 1.9	784 ± 12	96.4 ± 1.0
EVA/MWNT1200–10%–6 h	18.5 ± 1.4	589 ± 63	96.2 ± 1.0
EVA/MWNT–10%–6 h–TNBT	16.6 ± 0.4	679 ± 136	95.2 ± 1.0
EVA/MWNT800–10%–6 h–TNBT	19.5 ± 1.9	661 ± 57	95.0 ± 0.7
EVA/MWNT1000–10%–6 h–TNBT	19.9 ± 1.6	644 ± 52	95.8 ± 0.0
EVA/MWNT1200–10%–6 h–TNBT	19.6 ± 0.5	488 ± 34	95.6 ± 1.0

FTIR analysis of the saponified EVA and EVA/MWNT nanocomposites

The composition of the saponified EVA and its percentage saponification were determined from the FTIR absorbance ratio of the methyl group of the VAc unit (1370 cm^{-1}) and the methylene group of the ethylene unit (720 cm^{-1})[9] with eq. (1). The results are summarized in Table IV. After saponification for 6 h, the residual VAc content was 3.2%, and the percentage saponification reached 88.6%. It could be seen that the percentage saponification of EVA was not significantly changed after 6 h. This was because the saponification took place preferentially at the surface of the EVA particles and allowed the EVA molecules inside the particles to remain almost intact.[16]

Figure 11 shows FTIR spectra of the EVA/MWNT nanocomposites and their corresponding saponification times. The EVA was characterized by the presence of symmetric and asymmetric stretching vibrations of the CH_2 groups at 2750 and 2985 cm^{-1}, respectively. The bands occurring in the 1650–1775-cm^{-1} region resulted from the C=O stretching mode. The FTIR spectra of EVA/MWNTs–10% after saponification for 6 h indicated that some of the VAc units remained because the C=O stretching band still appeared at 1650–1775 cm^{-1}. The results indicate that the MWNTs did not affect the saponification of EVA molecules significantly.

DSC thermal properties of the saponified EVA and EVA/EB–MWNT nanocomposites

Figure 12 illustrates the DSC thermogram of the EVA and EVA/MWNT–10% nanocomposite as a function of the saponification time, and the measured thermal properties are summarized in Table V. EVA exhibited bimodal melting peaks at 58.3 and 73.8°C (Table V). The bimodal melting peaks of EVA also appeared similarly in the second-scan DSC thermogram. As the radical copolymerization of ethylene and VAc proceeded quite randomly because both the copolymerization reactivity ratios were close to 1.09, the bimodal melting peaks indicated that the reactor for the production of EVA was not a perfectly mixed system. The feeding of the monomers should have been realized in several reaction zones.[11]

As the saponification time increased, the melting temperature (T_m) of saponified EVA increased, and the crystallization peak in the course of cooling at −5°C/min from the melt state appeared at a higher temperature. As shown in Table V, the heat of crystallization (ΔH_c) also increased with the saponification time; this indicated that a possible intermolecular hydrogen bond between the VOH units favored the crystallization of the intervening segments composed of ethylene units. Saponification should have taken place mostly at the surface of the EVA coagulant. The lower melting peak of the first-scan DSC thermogram for EVA [Fig. 12(a)] at a short saponification time should have been due to the presence of unsaponified or less saponified EVA molecules inside the particles. The lower melting peak almost disappeared after 6 h of saponification time. The saponified EVA/MWNT1200–10% nanocomposite exhibited similar melting and crystallization behavior but T_{m2}, crystallization temperature (T_c), and ΔH_c of saponified EVA/MWNT1200–10% had lower values than those of corresponding saponified EVA. This suggested that the MWNTs hindered the diffusion and the rearrangement of polymer chains for crystallization when it had a 10 wt % content.

Thermal stability of the saponified EVA/MWNT nanocomposites

The investigation of the thermal stability of EVA and the saponified EVA/MWNTs was carried out with TGA under an N_2 atmosphere. As shown in Figure 13, EVA and EVA/MWNTs−10% showed the typical step degradation profile with the initial stage involving acetic acid evolution and the second involving main-chain degradation.[17,18] With the incorporation of 10 wt % pristine MWNTs, it was found that the degradation temperature at maximum improved from 450 to 500°C. Several articles have reported increases in the degradation temperature of

the polymer matrix with the addition of CNTs.[19,20] The enhancement in the decomposition temperature was attributed to the interaction between the polymer matrix and the CNTs. As the saponification time increased, the thermal stability of the EVA/MWNT nanocomposite increased significantly and almost showed one weight loss step. For EVA/MWNT1200–10%−6 h, the TGA traces showed a significant shift in weight loss toward higher temperatures with a stabilization at 50°C higher than that of EVA. An increase in the VOH units would raise the intermolecular interaction between EVOH molecules, and it would shorten the segment length of ethylene units in sequence. Such properties are caused by strong hydrogen-bond interactions, both intermolecular and intramolecular, which increase the thermal stability of the polymer chains and the high thermal stability of inorganic fillers.[16]

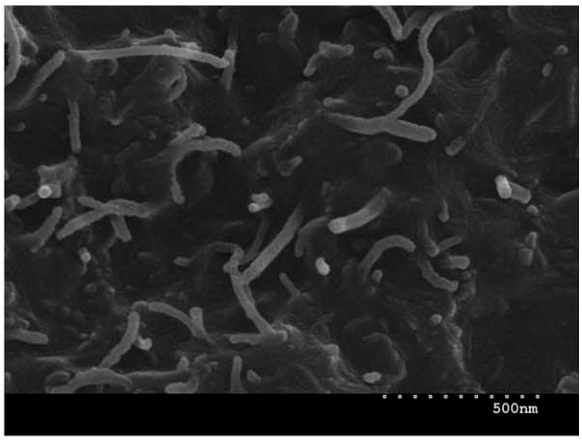

(a) EVA/MWNT1000-10%-0h

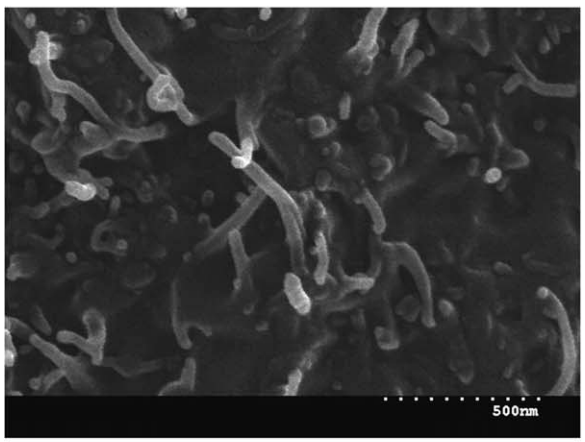

(b) EVA/MWNT1000-10%-6h

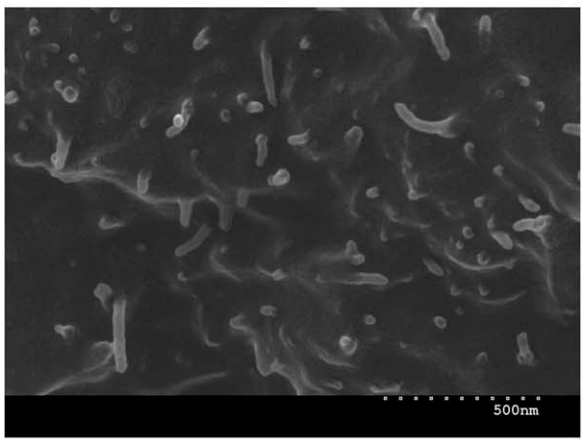

(c) EVA/MWNT1000-10%-6h-TNBT

Figure 14 Higher magnification SEM micrographs of the fractured EVA/MWNT1000–10% specimen surfaces after saponification for 6 h and the heterogeneous reaction in the presence of the TNBT catalyst for 20 min.

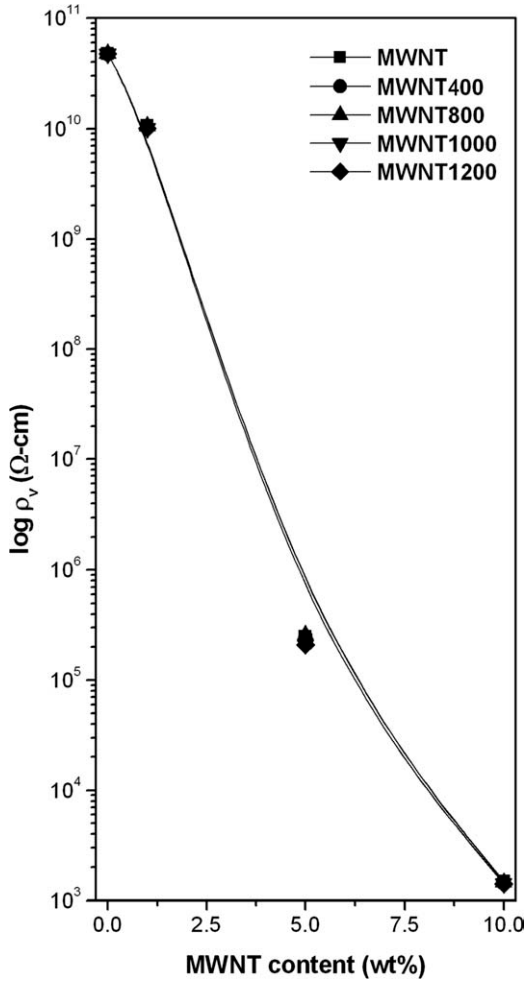

Figure 15 ρ_v changes of the EVA/EB–MWNT nanocomposites.

Tensile properties of the saponified EVA/MWNT nanocomposites

The tensile properties of the EVA/EB–MWNT nanocomposites after saponification for 6 h and heterogeneous reaction in the presence of TNBT catalyst for 20 min are demonstrated in Table VI. It was found that the tensile strength of the saponified

TABLE VII
ρ_v Changes of the EVA/EB–MWNT Nanocomposites with EB–MWNT Content

EB–MWNT content (wt %)	ρ_v (Ω cm $\times$ 10^{-5})				
	MWNT	MWNT400	MWNT800	MWNT1000	MWNT1200
0.0	474,600	474,600	474,600	474,600	474,600
2.5	107,083	107,013	104,900	100,983	100,271
5.0	2.48	2.48	2.46	2.10	2.10
10	0.0149	0.0149	0.0145	0.0143	0.0141

nanocomposite samples was significantly increased compared to that of EVA. The addition of 10 wt % pristine MWNTs enhanced the tensile strength of EVOH by 158%, whereas the addition of MWNT800, MWNT1000, and MWNT1200 increased it by 177, 171, and 175%, respectively. It was obvious that the EB irradiation of the filler resulted in better adhesion because of enhanced interactions between the EB–MWNTs and the polymer matrix. Further increases in the tensile strength by about 4% through heterogeneous reaction in the presence of TNBT in dimethyl sulfoxide could be explained in terms of the homogeneous distribution and interfacial bonding of the EB–MWNTs with the matrix, which helped with effective load transfer.

Figure 14 shows higher magnification SEM micrographs of the fractured surface of EVA/MWNT1000–10% after saponification for 6 h and heterogeneous reaction in the presence of TNBT catalyst for 20 min. For EVA/MWNT1000–10%–6h [Fig. 14(b)] and EVA/MWNT1000–10%–6h–TNBT [Fig. 14(c)], we found that the MWNTs dispersed well in the EVOH matrix. Most of the MWNTs were broken in the interface rather than pulled out from the polymer matrix. However, the EVA/MWNT1000–10% specimen showed a different morphology [Fig. 14(a)]. Most of the MWNT fibers were pulled out from the EVA matrix. Such a discrepancy demonstrated that a stronger interfacial adhesion existed between the MWNTs and the EVOH matrix. Moreover, some polymer chains were just physically blended with the MWNTs. All of the observations of the fracture surfaces were in accordance with the mechanical properties discussed previously.

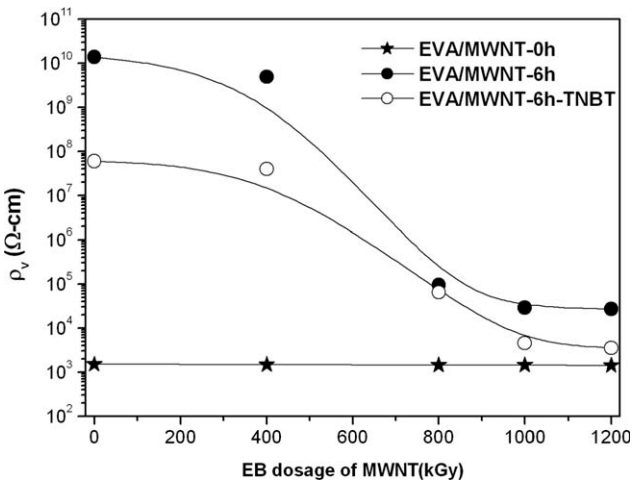

Figure 16 ρ_v changes of the saponified EVA/EB–MWNT nanocomposites.

ρ_v changes of the saponified EVA/EB–MWNT nanocomposites

Figure 15 shows a rapid decrease in ρ_v of the EVA/EB–MWNT nanocomposites with increasing MWNT content, as shown in Table VII. This rapid decrease was characteristic of the loading level at which the MWNT particles began to come into contact with one another to form a conductive network. As the MWNT particles were loaded in a polymer matrix over a percolation threshold concentration, the nanocomposite became an electrical conductor at room temperature. The percolation threshold of the EVA/MWNT nanocomposites formed by solution mixing was approximately 5 wt %; this was due to the advantageous effect of composites with higher aspect ratios compared with spherical or elliptical fillers in the formation of conducting networks in the polymer matrix.

However, ρ_v of nanocomposites was not significantly changed with irradiation dose (Table VII).

After saponification for 6 h, the ρ_v values of the hot-pressed EVA/MWNT and EVA/EB–MWNT nanocomposites increased significantly compared to those of its unsaponified ones (Fig. 16). The ρ_v increments of pristine MWNTs containing nanocomposite were more conspicuous than those of the EB–MWNTs. This indicated that the EVOH/MWNT nanocomposites had less electrically conductive surfaces because the MWNT fibers were mostly trapped inside the matrix polymer. Thereby, the reduction of ρ_v at higher irradiation does and after heterogeneous reaction could have been explained in terms of the enhanced distribution of MWNTs through the EVOH matrix, which helped with effective electroconductive surface formation.

CONCLUSIONS

EVOH/MWNT nanocomposite particles were successfully prepared by the precipitation of a EVA/

EB–MWNT/toluene suspension in an ethanol/KOH solution. The MWNTs were functionalized by EB irradiation in air at room temperature. The nanocomposite particles had a spongelike structure of the connected matrix polymer and MWNTs. At low EVA/MWNT concentrations, the particles were less porous, and the precipitated polymer phase had a granular structure. At high concentrations, the void porosity was increased, and the precipitated polymer phase became a spongelike structure.

The TGA thermogram of EVA showed the typical step degradation profile with the initial stage involving acetic acid evolution and the second stage involving main-chain degradation. As the saponification time increased, the thermal stability of the EVA/MWNT nanocomposite increased significantly and almost showed one weight loss step. An increase in VOH units raised the intermolecular interaction between the EVOH molecules and increased the thermal stability of the polymer chains.

A significant improvement in the tensile strength of the EVOH nanocomposites was obtained with EB–MWNTs compared to that with the pristine MWNTs. It was obvious that EB irradiation of filler resulted in better adhesion because of the enhanced interactions between the MWNTs and the polymer matrix. Because the nanocomposite filler prepared by this method was highly porous and had good hydrophilicity, good mechanical strength, and good thermal properties, it could be used for industrial applications, such as polymeric fillers in aqueous system, electroconductive materials, and thin-film membranes.

References

1. Pérez, E.; Lujan, M.; Salazar, J. M. Macromol Chem Phys 2000, 201, 1323.
2. Ramakrishnan, S. Macromolecules 1991, 24, 3753.
3. Lasagabaster, A.; Abad, M. J.; Barral, L.; Ares, A. Eur Polym J 2006, 42, 3121.
4. Ramanathan, T.; Fisher, F. T.; Ruoff, R. S.; Brinson, L. C. Chem Mater 2005, 17, 1290.
5. Park, E. S. J Appl Polym Sci 2007, 105, 460.
6. Kim, G. T.; Park, E. S. J Appl Polym Sci 2008, 109, 1381.
7. Zhao, C.; Yang, K.; Zhou, X.; Lei, Y.; Yang, G.; Lei, Y.; Nishi, N. Colloid J 2005, 67, 140.
8. Baker, R. W. Membrane Technology and Applications, 2nd ed.; Wiley: Chichester, United Kingdom, 2004.
9. Parker, J. R.; Waddell, W. H. J. Elastomer Plast 1996, 28, 140.
10. Lau, K.-T.; Hui, D. Compos B 2002, 33, 263.
11. Thostenson, E. T.; Zhifeng, R.; Chou, T. W. Compos Sci Technol 2001, 6, 1899.
12. Maazouz, A.; Sautereau, H.; Gerard, J. F. J Appl Polym Sci 1993, 50, 615.
13. Banerjee, S.; Hemraj-Benny; T.; Wong, S. S. Adv Mater 2005, 17, 17.
14. Radovic, L. R. Chemistry and Physics of Carbon; Marcel Dekker: New York, 2003.
15. Kong, H.; Gao, G.; Yan, D. J Am Chem Soc 2004, 126, 412.
16. Park, E. S.; Kim, M. N.; Yoon, J. S. J Polym Sci Part B: Polym Phys 2002, 40, 2561.
17. Allen, N. S.; Edge, M.; Rodriguez, M.; Liauw, C. M.; Fontan, E. Polym Degrad Stab 2001, 71, 1.
18. McGrattan, B. J Appl Spectrosc 1994, 48, 1472.
19. Yang, J.; Lin, Y. H.; Wang, J. F.; Lai, M. F.; Li, J.; Liu, J. J.; Tong, X.; Cheng, H. M. J Appl Polym Sci 2005, 98, 1087.
20. Costache, M. C.; Wang, D. Y.; Heidecker, M. J.; Manias, E.; Wilkie, C. A. Polym Adv Technol 2006, 17, 272.